Journal of Porous Materials (2020) 27:1329–1337
https://doi.org/10.1007/s10934-020-00905-0

Controllable synthesis of ZSM-11/ZSM-5 intergrowth zeolite using 1,3-cyclohexanedimethanamine as organic template

Zhendong Wang[1] · Yi Luo[1] · Xiangcheng Li[1] · Weimin Yang[1]

Published online: 2 June 2020

Abstract
A new organic template, 1,3-cyclohexanedimethanamine (1,3-CDA), is found to be effective in directing the crystallization of ZSM-11 zeolite. Phase transformation from ZSM-11 to ZSM-5 was observed when varying the molar ratios of OH^-/SiO_2, Na^+/SiO_2 and SiO_2/Al_2O_3. ZSM-11/ZSM-5 intergrowth zeolites with ZSM-5 contents from 10 to 100% were synthesized. The structural intergrowth was evidenced by TEM, and its formation may be ascribed to the competition between ZSM-11 and ZSM-5 zeolite in the system. The morphology of zeolite varies with the change of composition of the starting gel. The particle sizes of the products decrease with the increase of 1,3-CDA/SiO_2 and Na^+/SiO_2 ratios. With the increase the OH^-/SiO_2 ratio, the sizes decrease at first and then increase. Meanwhile, the morphologies change from cross-like aggregates of orthotropic rods to aggregates of nano-rods, and then to irregular bulk crystals. With the decrease of SiO_2/Al_2O_3 ratios from 100 to 40, the particle sizes decrease from 200 to about 50 nm, resulting in the formation of nanosized ZSM-11/ZSM-5 intergrowth zeolite.

Keywords ZSM-11 · ZSM-5 · Intergrowth zeolite · 1,3-Cyclohexanedimethanamine · Morphology

1 Introduction

Zeolites are important microporous crystalline materials and have been found applicable in a wide range of areas, such as catalysis, adsorption, separation, and ion-exchange [1]. Since the pioneering work by Barrer in the early 1960s [2], numerous organic compounds, usually known as the structure-directing agents (SDAs) or organic templates, have been extensively used for the synthesis of novel zeolites and related microporous materials [3, 4]. Up to now, it is still the most important and effective way to obtain materials with new pore structures, morphologies and/or properties. Recently, research on the preparation of intergrowth zeolites has drawn much attention, because the combination of two structural phases may offer possibilities to obtain better adsorbents and catalysts [5–7]. Seeking for the special properties of those materials has motivated the discovery of a series of zeolites with intergrowth structures, such as zeolite beta [8], **MTT/TON** [9], **EMT/FAU** [10], **RTH/ITE** [11], **CHA/AEI** [12], and **ERI/OFF** [13]. A multitude of studies have illustrated that the precondition for the formation of these zeolitic materials is that the intergrown frameworks should have at least part of or all of the basic structure building units in common [14].

ZSM-5 (**MFI**) and ZSM-11 (**MEL**) zeolites are very important members of the pentasil zeolite family. The framework structures of these two zeolites are closely related to each other and they can be depicted using a stacking manner of pentasil sheets. The adjacent pentasil sheets of **MFI** structure are related to one another by an inversion manner, while those of **MEL** structure are connected by mirror symmetry [15, 16]. The minor difference in pore structure makes possible the preparation of ZSM-11/ZSM-5 intergrowth zeolite, which was first reported by Mobil Oil Corporation in 1979 [17]. Since then, it has become an attractive research object for its unique catalytic and adsorptive properties. At present, ZSM-11/ZSM-5 intergrowth zeolite has been commercialized in ethylbenzene production through vapor-phase alkylation of benzene with FCC off-gas [18]. Meanwhile, it also

✉ Zhendong Wang
wangzd.sshy@sinopec.com

✉ Weimin Yang
yangwm.sshy@sinopec.com

[1] State Key Laboratory of Green Chemical Engineering and Industrial Catalysis, Sinopec Shanghai Research Institute of Petrochemical Technology, Shanghai 201208, China

shows excellent catalytic properties in n-decane cracking [7] and methanol to hydrocarbons reactions [6].

For the preparation of intergrowth zeolite, the key point is the formation of two different structures in one synthetic system at the same time. So, competitive hydrothermal synthetic system is usually utilized, which contains two structure-directing agents (two organic templates or alkali cations) [19, 20]. Each template facilitates the crystallization of one structure. ZSM-11/ZSM-5 intergrowth zeolite is most commonly synthesized in such system using binary organic templates of tetrabutylammonium (TBA) and tetrapropylammonium (TPA). However, the content of ZSM-11 can hardly be tuned due to the dominating formation of the **MFI** structure. The **MEL** structure would not appear until the content of TBA was greater than 90%, but there still exists a great amount of **MFI** in the final product even the relative amount of TBA is higher than 98% [21]. It is of great desire to develop an effective strategy for the synthesis of ZSM-11/ZSM-5 intergrowth zeolite with adjustable content of the ZSM-11 phase. Compared with quaternary ammonium cations, some templates such as amines, which result in various zeolite topologies, possess better molecular flexibility and display a less specific relationship with synthesized products [22–24]. Therefore, using amines as templates to construct a competitive crystallization system for the synthesis of intergrowth zeolites may show advantage in tuning the compositions of intergrowth zeolites due to their relatively weak templating effects.

Herein, a brand new organic template, 1,3-cyclohexanedimethanamine (1,3-CDA), was used to synthesize ZSM-11/ZSM-5 intergrowth zeolite. The composition and morphology of the intergrowth zeolite can be easily controlled by varying the initial OH^-/SiO_2 and SiO_2/Al_2O_3 ratios of the reaction mixture.

2 Experimental

2.1 Zeolite synthesis

ZSM-11/ZSM-5 intergrowth zeolite was synthesized by hydrothermal crystallization using silica sol (40 wt% SiO_2, Jiangyin LDK technology & trade Co., Ltd.), sodium hydroxide (96.0 wt%, China Medicine (Group) Shanghai Chemical Reagent Co., Ltd.), sodium aluminate (43 wt% Al_2O_3, 35 wt% Na_2O, Zibo Lier Chemical Co. Ltd.), sodium chloride (99.5 wt%, China Medicine (Group) Shanghai Chemical Reagent Co. Ltd.), 1,3-CDA (99 wt%, TCI shanghai) and distilled water as starting materials. The samples synthesized under different crystallization conditions are listed in Table 1. The typical procedure for the synthesis of ZSM-11/ZSM-5 intergrowth was as follows: NaOH, $NaAlO_2$, NaCl (if necessary) and 1,3-CDA were successively added into deionized water under stirring until they were dissolved thoroughly, and then the silica sol was added dropwise. And the starting mixture was obtained after 30 min's stirring at room temperature. ZSM-11 zeolite synthesized using tetrabutylammonium bromide (TBABr, 99 wt%, Shanghai Chemical Reagent Co., Ltd.) as an organic template was used as the reference sample. The molar composition of the

Table 1 The products synthesized using 1,3-CDA as organic templates under various conditions

Run	SiO_2/Al_2O_3	OH^-/SiO_2	1,3-CDA/SiO_2	H_2O/SiO_2	$NaCl/SiO_2$	Products	ZSM-5 contents[a]	Particle size (μm)[b]
1	70	0.09	0.20	25	0	Amorphous	–	–
2	70	0.09	0.30	25	0	ZSM-11/ZSM-5	< 10%	2.0 × 2.0 × 1.5[c]
3	70	0.09	0.40	25	0	ZSM-11/ZSM-5	< 10%	1.6 × 1.6 × 0.95
4	70	0.09	0.50	25	0	ZSM-11/ZSM-5	< 10%	1.0 × 1.0 × 0.56
5	70	0.08	0.30	25	0	Amorphous	–	–
6	70	0.15	0.30	25	0	ZSM-11/ZSM-5	20%	0.5
7	70	0.18	0.30	25	0	ZSM-11/ZSM-5	50%	0.2
8	70	0.35	0.30	25	0	ZSM-5	100%	0.8
9	70	0.09	0.30	25	0.03	ZSM-11/ZSM-5	10%	1.8 × 1.8 × 1.2
10	70	0.09	0.30	25	0.09	ZSM-11/ZSM-5	15%	1.5 × 1.5 × 1.0
11	30	0.18	0.30	25	0	Amorphous	–	–
12	40	0.18	0.30	25	0	ZSM-11/ZSM-5	20%	0.06
13	60	0.18	0.30	25	0	ZSM-11/ZSM-5	30%	0.08
14	100	0.18	0.30	25	0	ZSM-5 + magaditte	–	4.5 × 4.5 × 2.5

[a]Estimated from the X-ray diffraction data

[b]Determined from the SEM images

[c]length × length × thickness of cross-like particles

starting mixture for its synthesis was 1 SiO_2:1/70 Al_2O_3:0.06 Na_2O:0.20 TBABr:25 H_2O.

All of the above reaction mixtures were subsequently transferred into teflon-lined stainless steel autoclaves and crystallized dynamically (20 rpm) at 150 °C under autogenous pressure for 3 days. When the crystallization was over, the autoclaves were quenched using cold water and the samples were separated by centrifugation, washed using deionized water, and dried at 110 °C for 12 h. Finally, the organic template was removed by calcination at 550 °C for 5 h in air.

2.2 Characterization

X-ray powder diffraction (XRD) patterns were recorded on a D8 Advance SS X-ray diffractometer using CuKa radiation, operating at 40 kV and 40 mA. The data were collected from 2° to 50° with a sampling interval of 0.020° at a scanning rate of 5°/min. Quantification of the ZSM-5 content in the ZSM-11/ZSM-5 intergrowth structure was carried out by comparing the experimental XRD patterns with the simulated patterns [7, 25]. Scanning electron microscopy (SEM) images are taken on a field emission XL30E scanning electron microscopy (FEI Company). Surface areas and pore volumes were obtained from N_2 adsorption/desorption isotherms using multipoint BET and t-plot methods. Prior to analysis, each sample was degassed under vacuum at 350 °C for 10 h. The experiments were performed on Micromeretic ASAP2020M physisorption apparatus at a liquid nitrogen temperature of −196 °C. The SiO_2/Al_2O_3 molar ratios of crystal samples were quantified by inductively coupled plasma (ICP) on a Varian 725-ES instrument. The solid state ^{27}Al MAS-NMR measurements were performed on a Bruker Avance III 400 MHz spectrometer at 104.26 MHz. All samples were fully hydrated before ^{27}Al MAS-NMR studies. The TGA curves were obtained by a SDT Q600 V20.9 Build 20 thermal analyzer. Samples were exposed to air atmosphere where temperature was elevated from 30 to 900 °C at a rate of 10 °C/min.

3 Results and discussion

3.1 Influence of the 1,3-CDA/SiO_2 ratio on the synthesis of ZSM-11/ZSM-5 intergrowth zeolite

Previous literatures [26–28] have reported that the reflection peaks at 2θ of 7.92°, 8.78°, 23.14°, 23.98° and 45.20° are typical characteristic peaks of ZSM-11 zeolite. It is believed that when two peaks appeared at 2θ of 22.4–24.8° and single peak occurred at 2θ of 45.2°, the ZSM-11 framework is free of ZSM-5 [29]. Therefore, ZSM-11 zeolites synthesized with TBA^+ cations were always seen as pure phase in most works. However, Davis et al. [30] have demonstrated that those materials are actually ZSM-11/ZSM-5 intergrowth zeolites (ZSM-5 content < 5% [19]). Because the XRD patterns of those materials are absent of reflection peaks of (110) and (330), and companied with a shoulder peak appeared at 2θ range of 22.4–24.8°. In principle, the X-ray diffraction of pure ZSM-11 is much different from that of pure ZSM-5 in 2θ range of 22.4–24.8° and 44.5–46.0° (differences in these regions are shown in Table 2). To facilitate the comparison and discussion, diffraction peaks at 2θ region of 22.4–24.8° and 44.5–46.0° are presented as insert.

The influence of the organic template content on products was studied by changing the molar ratio of 1,3-CDA to SiO_2 (1,3-CDA/SiO_2) in the reaction mixture. The composition of starting gel was: 1 SiO_2:1/70 Al_2O_3:0.045 Na_2O:x 1,3-CDA:25 H_2O, where x = 0.2, 0.3, 0.4 and 0.5 (runs 1–4 in Table 1). Figure 1 shows the XRD patterns of the reference sample synthesized with TBABr (Fig. 1a) and samples prepared using 1,3-CDA with different 1,3-CDA/SiO_2 molar ratios (Fig. 1b–d). It can be seen that the XRD patterns in the 2θ region of 22.4–24.8° (Fig. 1b) and 44.5–46.0° (Fig. 1c) of products synthesized with 1,3-CDA compare well with the pattern of the reference sample synthesized using TBABr, which was regarded as the pattern of pure ZSM-11 zeolite (absent (110) and (330) reflections). Typical (501), (303) and (10,0,0) reflections attributed to ZSM-11 were expected to be presented in those regions. Though the (051), (151), (133) and (0,10,0) reflections associated with **MFI** structure do not appear, a shoulder peak in the 2θ region of 22.4–24.8° is visible. Therefore, products synthesized using 1,3-CDA

Table 2 Reflections of different planes of ZSM-5 and ZSM-11 occurred at 2θ = 22.4–24.8° and 44.5–46°

Zeolite		2θ = 22.4–24.8°					2θ = 44.5–46.0°	
ZSM-5	2θ	23.2	23.3	23.7	24.0	24.4	45.3	45.6
	hlk	501	051	151	303	133	10,0,0	0,10,0
ZSM-11	2θ	23.1	–	–	23.9	–	45.2	–
	hlk	501	–	–	303	–	10,0,0	–

Data collected from "Collection of Simulated XRD Powder Patterns for Zeolites"

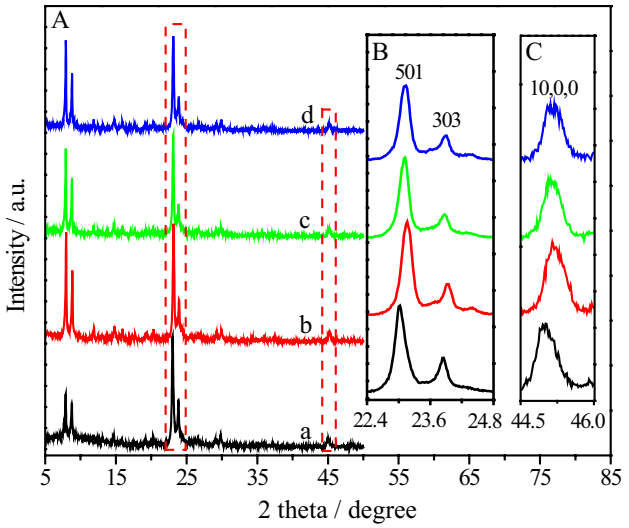

Fig. 1 XRD patterns of reference sample synthesized with **a** TBABr and samples prepared using 1,3-CDA as templates with different 1,3-CDA/SiO_2 ratios of **b** 0.3, **c** 0.4, **d** 0.5

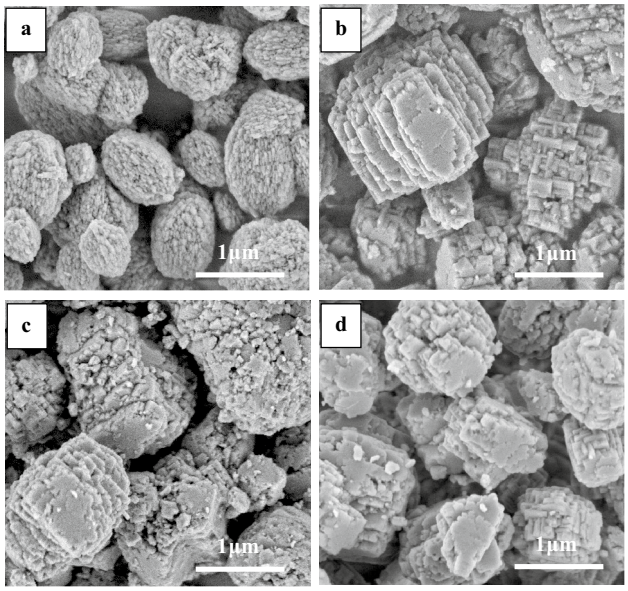

Fig. 2 SEM images of the reference sample synthesized with **a** TBABr and samples prepared using 1,3-CDA as templates with different 1,3-CDA/SiO_2 ratios of **b** 0.3, **c** 0.4, **d** 0.5

are typical ZSM-11/ZSM-5 intergrowth zeolite, the same as that synthesized using TBABr. With the increase of 1,3-CDA/SiO_2 from 0.3 to 0.5, there is no obvious change in the XRD patterns, and the ZSM-5 contents of ZSM-11/ZSM-5 intergrowth zeolites are less than 10%. However, when the 1,3-CDA/SiO_2 ratio is less than 0.3, the obtained product is amorphous (run 1 of Table 1). Synthesis of pure ZSM-11 zeolite using 1,3-CDA was also carried out. Unfortunately, only ZSM-11/ZSM-5 intergrowth zeolites were obtained. As reported previously, pure ZSM-11 zeolite is difficult to be synthesized [30]. Up to now, 2,2-diethoxyethyltrimethylammonium hydroxide and 3,5-dimethylpiperidinium derivatives are the only two organic templates that are claimed to be efficient in the synthesis of pure ZSM-11 zeolite [30].

Figure 2 shows the SEM images of samples synthesized using TBABr and 1,3-CDA. All the products are well crystallized zeolites, and no obvious amorphous phase and impurities are observed, which indicates that the obtained materials are intergrowths of ZSM-11 and ZSM-5, not physical mixtures. The morphologies of ZSM-11/ZSM-5 intergrowth zeolites synthesized using 1,3-CDA as template are all cross-like aggregates of bulk crystals, and the crystals interact with one another in an orthotropic manner (Fig. 2b–d). Unlike the crystallizations following an 'oriented attachment pathway' with the addition of organic growth modifiers [31] or organosilane [32], here the aggregations of small crystals may follow a random, not oriented, pathway. The reference sample synthesized with TBABr is aggregates of nano-zeolite crystals with spindle-like shape (Fig. 2a). With the increase of 1,3-CDA/SiO_2 ratio, the outlines of the cross-like particles became a little indistinct. In the meanwhile, a decrease in crystal length from 2 to 1 μm was observed. The texture properties of ZSM-11/ZSM-5 zeolite (run 2) derived from N_2 adsoption-desorption test are listed in Table 3. Its surface area and microporous volume are 346 m^2/g and 0.13 cm^3/g, respectively.

TGA curves of the as-made ZSM-11/ZSM-5 intergrowth zeolites synthesized using TBABr and 1,3-CDA (run 2) are shown in Fig. 3. The total weight loss of ZSM-11/ZSM-5 synthesized using 1,3-CDA (11.97%) is less than that of TBABr (14.43%) from room temperature to 700 °C. The weight loss below 200 °C is assigned to adsorbed water, and the loss from 200 to 700 °C corresponds to the decomposition of the organic species. The data originated from TGA is presented in Table 4. The average number of organic molecules per unit cell (R/u.c.) of ZSM-11/ZSM-5 intergrowth zeolite was calculated by thermal analysis [33]. The numbers of H_2O/u.c. and TBABr/u.c. of the reference sample are 7.3 and 2.7, respectively. They are in good agreement with the data reported in previous work [33]. Meanwhile, the numbers of H_2O/u.c. and 1,3-CDA/u.c. of Run 2 are 6.9 and 4.7, respectively. It shows that the number of H_2O/u.c of the reference sample is almost the same as that of ZSM-11/ZSM-5 (run 2). The number of R/u.c. of run 2 is nearly twice as many as that of the reference sample synthesized using TBABr. TBA^+ cations balanced some of the framework charges derived from the incorporations of Al into the framework. When 1,3-CDA was used, the organic molecule mainly acted as pore filler, and almost all the framework charges were balanced by Na^+ cations.

These results indicate that well crystallized ZSM-11/ZSM-5 intergrowth zeolite (ZSM-5 content < 10%) can be

Table 3 Texture properties of ZSM-11/ZSM-5 intergrowth zeolites

Samples	SiO_2/Al_2O_3		S_{BET}[b] (m^2/g)	S_{micro}[b] (m^2/g)	S_{ext}[b] (m^2/g)	V_{micro}[b] (cm^3/g)
	Gel	Product[a]				
run 12	40	32	351	236	115	0.12
run 13	60	47	363	255	108	0.12
run 7	70	54	350	249	101	0.12
run 2	70	65	346	267	78	0.13

[a]Given by ICP

[b]Given by N_2 adsorption

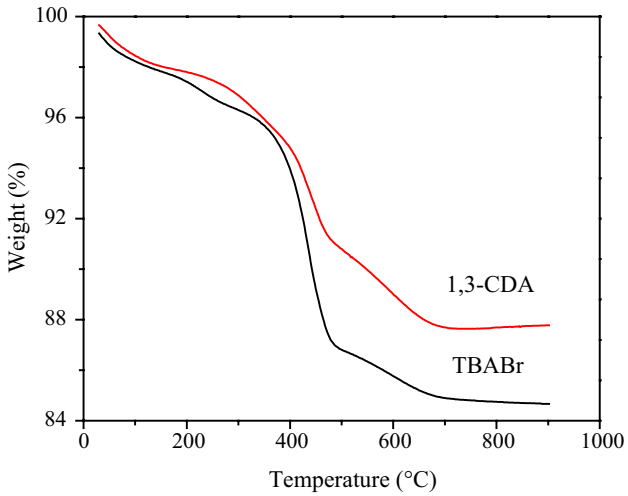

Fig. 3 TGA carves of ZSM-11/ZSM-5 intergrowth zeolites synthesized using 1,3-CDA and TBABr

synthesized using 1,3-CDA as an organic template with a wide range of 1,3-CDA/SiO_2 molar ratios. The increase in 1,3-CDA/SiO_2 ratio didn't exhibit obvious effects on the composition of the final products. On the contrary, it would facilitate the nucleation of ZSM-11/ZSM-5 and result in the decrease in the particle size.

3.2 Influence of the OH^-/SiO_2 and Na^+/SiO_2 ratios

The alkalinity of the reaction mixture has a dramatic influence on the nucleation and crystallization of silicon-aluminum zeolites. With the increase of hydroxide concentration, the numbers of silicate species such as monomers, liner and branched polymers increased, and the manner of polymerization between silicate species and aluminate species was consequently changed during the crystallization [34–36]. Herein different amounts of sodium hydroxide were used to evaluate the effect of OH^-/SiO_2 molar ratio on the crystallization of ZSM-11/ZSM-5. However, the addition of sodium hydroxide not only provides OH^- anions but also introduce Na^+ cations. In order to eliminate the interference of Na^+ cations, which may act as a structure-directing agent and/or charge-balancing agent [37–39] in the nucleation process of zeolites, NaCl was added. Moreover, crystallizations with different NaCl content but constant OH^-/SiO_2 ratio were also carried out to investigate the influence of Na^+/SiO_2 ratio.

XRD patterns of samples prepared with different OH^-/SiO_2 and Na^+/SiO_2 ratios are presented in Fig. 4A. When the OH^-/SiO_2 molar ratio is less than 0.09, the obtained products is amorphous (run 5 of Table 1). With the increase of OH^-/SiO_2 ratio from 0.09 to 0.35, diffraction peaks corresponding to (051), (151), (133) and (0,10,0) facets of **MFI** structure began to emerge and the intensities gradually increased (Fig. 4B(a–d)). The evolution of the diffraction peaks indicated the changes in the amount of ZSM-5 component. As exhibited in Table 1 (run 2,6–8), the percentages of ZSM-5 intergrowth in the ZSM-11/ZSM-5 intergrowth zeolite increased dramatically from 10 to 100% with the increase of OH^-/SiO_2 ratio. The reason may lie in the fact that the alkali condition facilitates the crystallization of **MFI** structure, since the attempt to synthesize ZSM-5 zeolite in organic template free system was successfully carried out under high alkali conditions [38, 40, 41]. In the synthesis of ZSM-11/ZSM-5 intergrowth zeolite using 1,3-CDA as templates, OH^- and Na^+

Table 4 ICP and TGA analysis of ZSM-11/ZSM-5 intergrowth zeolites synthesized using TBABr and 1,3-CDA

Zeolite precursor		ICP analysis (Products)		TGA analysis			
Organic template	SiO_2/Al_2O_3 (start gel)	SiO_2/Al_2O_3	Si/Na	H_2O content		R content	
				Wt. loss (%)	Mol./u.c.	Wt. loss (%)	Mol./u.c.
TBABr	70	67.5	67.1	1.9	7.3	12.5	2.7
1,3-CDA	70	65.4	135.5	1.9	6.9	10.1	4.7

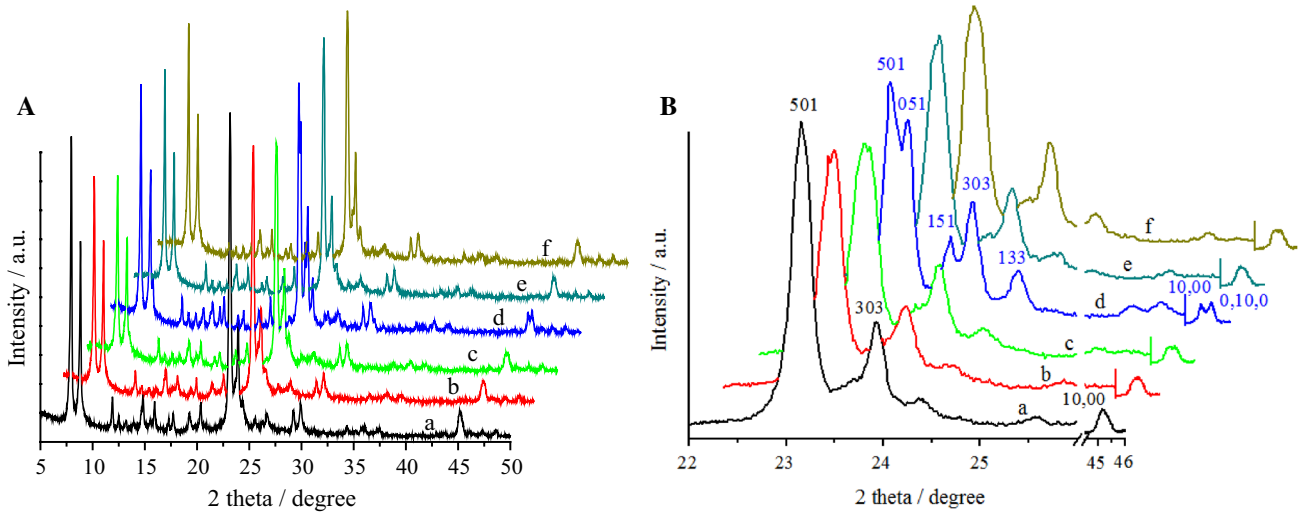

Fig. 4 **A** XRD patterns of ZSM-11/ZSM-5 intergrowth zeolites synthesized with different OH^-/SiO_2 (x) and $NaCl/SiO_2$ (y) ratios of (a) x = 0.09, y = 0, (b) x = 0.15, y = 0, (c) x = 0.18, y = 0, (d) x = 0.35, y = 0, (e) x = 0.09, y = 0.03 and (f) x = 0.09, y = 0.09. **B** Enlarged 2θ region around 22.4–24.8° and 44.5–46.0° of XRD patterns of ZSM-11/ZSM-5 intergrowth zeolites synthesized with different OH^-/SiO_2 (x) and $NaCl/SiO_2$ (y) ratios of (a) x = 0.09, y = 0, (b) x = 0.15, y = 0, (c) x = 0.18, y = 0, (d) x = 0.35, y = 0, (e) x = 0.09, y = 0.03 and (f) x = 0.09, y = 0.09

may also facilitate the crystallization of **MFI** structure. The competitive templating effect may be responsible for the formation of ZSM-11/ZSM-5 intergrowth zeolite, so that the amount of **MFI** phase increased with the rise of alkalinity.

When NaCl was added (run 9 and 10 in Table 1), the crystallization of ZSM-11/ZSM-5 intergrowth zeolites was not significantly affected, and no obvious changes were observed in the XRD patterns (Fig. 4B(e, f)). Figure 5 shows the SEM images of the obtained samples and different morphologies are exhibited. ZSM-11/ZSM-5 intergrowth zeolites (run 2, 6 and 7 in Table 1) are large aggregates of nano-crystals, and the nano-crystals seem like perpendicular to each other. With the increase of OH^-/SiO_2 ratio from 0.09 to 0.18, the size of the aggregates gradually decreased. The morphology of ZSM-5 zeolite (run 8, $OH^-/SiO_2 = 0.35$) differs significantly to ZSM-11/ZSM-5. As shown in Fig. 5d, the shape of the crystals is irregular, while the size is about 200–500 nm. When extra NaCl was introduced into the synthetic system, no obvious changes were observed from the SEM images (Fig. 5a, e, f) except for a slight decrease in the size of nano-crystals that formed the aggregates.

Alkalinity and sodium cations would influence the rates of nucleation and crystal growth during hydrothermal crystallization, which in turn would cause morphology diversity. Therefore, it would be effective to obtain various morphologies through proper control of alkalinity and sodium cations (especially alkalinity) [20, 42, 43]. Herein, the amount of ZSM-5 component of the ZSM-11/ZSM-5 intergrowth zeolites increased with the increase of OH^-/SiO_2, while the size of the nano-crystals decreased with the rise of alkalinity and Na^+ content.

3.3 Influence of SiO_2/Al_2O_3 molar ratio

Based on the typical crystallization mechanism of zeolite stated previously, the aluminum has great influence on the crystallization of zeolite [20, 44]. Therefore, the influence of SiO_2/Al_2O_3 molar ratio on the crystallization of ZSM-11/ZSM-5 intergrowth zeolite was investigated. As shown in Table 1, when the SiO_2/Al_2O_3 is lower than 30 (run 11), only amorphous product is produced, When the ratio is higher than 100 (run 14), ZSM-5 zeolite together with magadiite impurity (Fig. 6d, marked with asterisks) is obtained. As for SiO_2/Al_2O_3 ratio in the range of 40–70 (runs 12,13,7), all samples show typical diffraction peaks corresponding to ZSM-11/ZSM-5 intergrowth structures (Fig. 6a–c), which means that the proper SiO_2/Al_2O_3 molar ratio for the synthesis of ZSM-11/ZSM-5 ranges from 40 to 70. Differences in the intensities of the diffraction peaks can be clearly identified in the inserted parts As listed in Table 1, the amount of ZSM-5 increased from 20 to 50% with the increase of SiO_2/Al_2O_3 (Fig. 6b, c), indicating the differences in the amount of molar ratio from 40 to 70. It suggests that the reaction mixture with high SiO_2/Al_2O_3 molar ratio also facilitates the formation of **MFI** structure in the competitive crystallization system. This trend is highly consistent with those reported elsewhere before [45].

As the SEM images shown in Fig. 7, with the increase of SiO_2/Al_2O_3 molar ratio, ZSM-11/ZSM-5 intergrowth zeolites

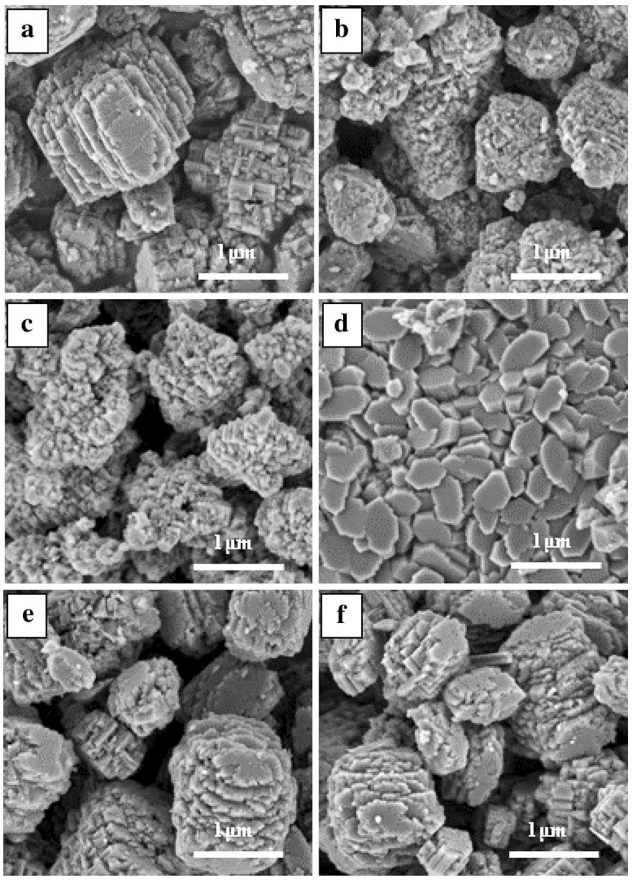

Fig. 5 SEM images of ZSM-11/ZSM-5 intergrowth zeolites synthesized with different OH^-/SiO_2 (x) and $NaCl/SiO_2$ (y) ratios of **a** x = 0.09, y = 0, **b** x = 0.15, y = 0, **c** x = 0.18, y = 0, **d** x = 0.35, y = 0, **e** x = 0.09, y = 0.03 and **f** x = 0.09, y = 0.09

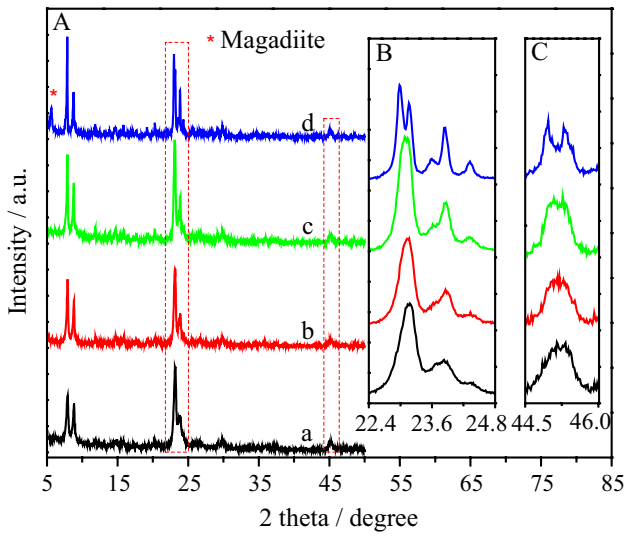

Fig. 6 XRD patterns of products synthesized with SiO_2/Al_2O_3 ratios of **a** 40, **b** 60, **c** 70 and **d** 100

with various morphologies are observed. Aggregates of nano-crystals and well-dispersed nano-crystals are obtained with lower SiO_2/Al_2O_3 molar ratios (Fig. 7a, b), while bulky aggregates of nano-rods are synthesized with higher SiO_2/Al_2O_3 molar ratios (Fig. 7c, d). The sizes of nano-crystals and bulky aggregates increase gradually with the increase of SiO_2/Al_2O_3 molar ratio. Interestingly, when the product was synthesized with $SiO_2/Al_2O_3 = 100$, the arrangement of the orthotropic rods in the cross-like aggregate was similar to that of the orthotropic channel system of **MEL**. Meanwhile, a few plate-like magadiite crystals were expected in the product. TEM images of the ZSM-11/ZSM-5 intergrowth crystal synthesized with SiO_2/Al_2O_3 ratio of 70 are presented in Fig. 7e. The intergrowth crystal is well crystallized, as indicated by the distinct lattice fringes. It is worth noting that some disorder regions of the lattice fringe are clearly observed at the edge of this crystal (marked by ellipses in Fig. 7e and enlarged image of Fig. 7f). As presented in Fig. 7g, the corresponding fast Fourier transform image of the disorder region (Fig. 7f) further indicates the intergrowth character of this crystal [16]. The TEM images and comparison of the experimental diffraction data provide compelling evidence for the intergrowth character of these materials.

Figure 8 showed the N_2 adsorption-desorption isotherms of samples synthesized with different Al contents. In addition to the typical adsorption behavior of microporous zeolites, N_2 adsorption also occurred at higher relative pressures, this may correspond to the inter-particle space of the zeolite aggregates of nano-crystals and was evidenced by the BJH pore size distribution in the region of 2–10 nm. The textural properties of ZSM-11/ZSM-5 intergrowth zeolites with different SiO_2/Al_2O_3 ratios are listed in Table 3. It is found that the SiO_2/Al_2O_3 ratio of the product is lower than that of the starting gel. This may result from the high alkalinity of the crystallization condition.

The ^{27}Al MAS-NMR spectra of all the ZSM-11/ZSM-5 samples synthesized with different SiO_2/Al_2O_3 molar ratios show clearly two sets of signals (Fig. 9): a broader band with a maximum at 54 ppm due to tetrahedrally coordinated framework Al and a low frequency signal around 0 ppm which is attributed to the extra-framework aluminum of octahedral coordination [46]. Although the amount of extra-framework aluminum showed a slightly increase with the decrease of SiO_2/Al_2O_3 ratio, most of the aluminum atoms in the synthesized zeolites were incorporated into the framework.

4 Conclusions

In summary, ZSM-11 zeolite and ZSM-11/ZSM-5 intergrowth zeolites with different morphologies and compositions were successfully synthesized using 1,3-CDA. The

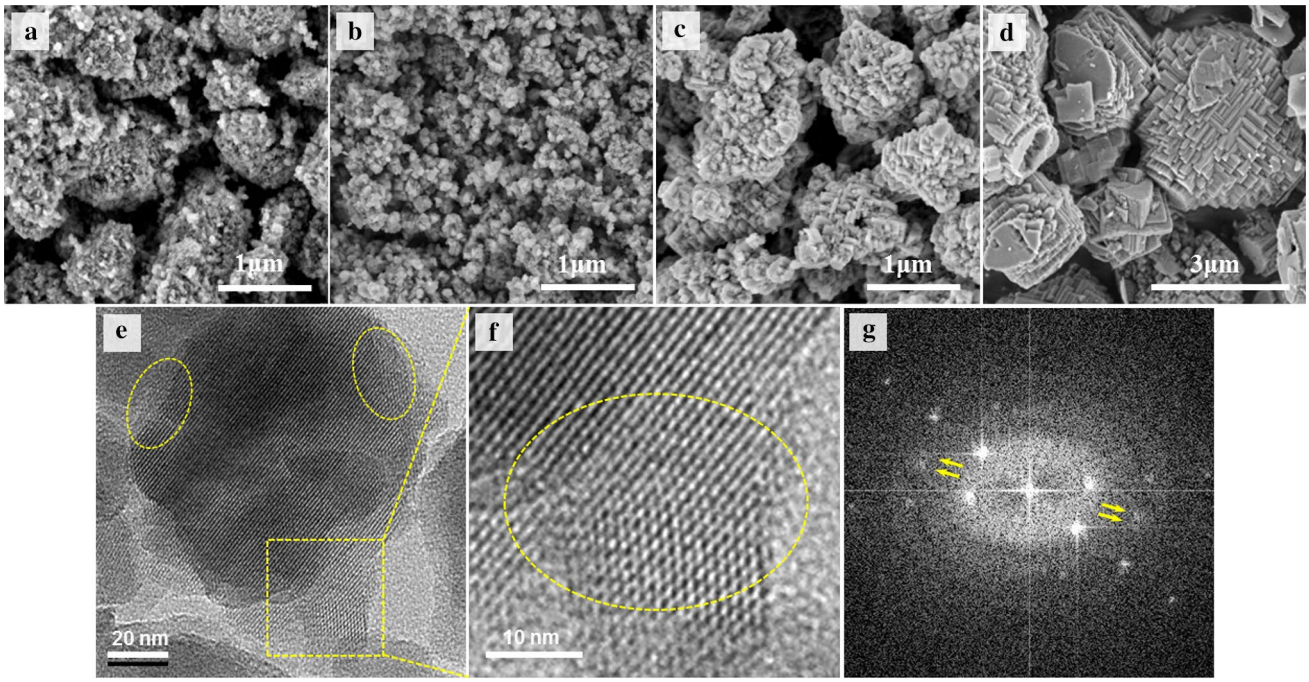

Fig. 7 SEM images of products synthesized with different SiO_2/Al_2O_3 ratios of **a** 40, **b** 60, **c** 70 and **d** 100. **e** TEM image of a ZSM-11/ZSM-5 intergrowth crystal synthesized with SiO_2/Al_2O_3 ratio of 70. **f** Enlarged TEM image of the intergrowth regions marked by a square in (**e**) shows obvious intergrowth boundary. **g** The corresponding fast Fourier transform image of (**f**)

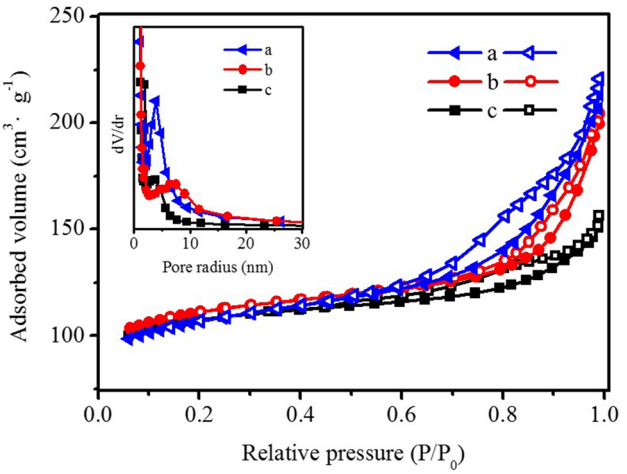

Fig. 8 N_2 adsorption-desorption isotherms and BJH desorption pore size distributions of ZSM-11/ZSM-5 intergrowth zeolites synthesized with different SiO_2/Al_2O_3 ratios of (a) 40, (b) 60 and (c) 70

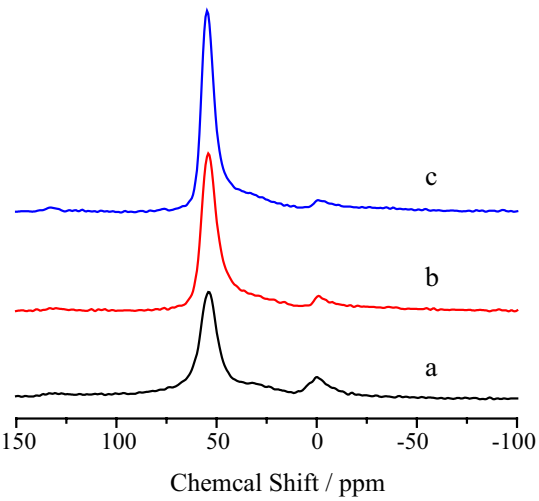

Fig. 9 ^{27}Al MAS-NMR spectra of products synthesized with SiO_2/Al_2O_3 ratios of (a) 40, (b) 60 and (c) 70

brand new organic template is more likely to direct the formation of ZSM-11 zeolite, while OH^- and Na^+ facilitate the formation of ZSM-5 zeolite. The competition between ZSM-11 and ZSM-5 may be responsible for the structural intergrowth.

Acknowledgements The authors gratefully acknowledge Dr. Jin-gang Jiang and Dr. Li Chen for their assistance with the NMR and TEM characterization, and Mr. Ruidan Liu for his help with improving the writing.

Funding This work was supported by the National Key R&D Program of China (2017YFB0702800), the National Natural Science Foundation

of China (21503280, 21972168), and China Petrochemical Corporation (Sinopec Group).

References

1. A. Corma, Chem. Rev. **95**, 559–614 (1995)
2. R.M. Barrer, P.J. Denny, J. Chem. Soc. **201**, 983–1000 (1961)
3. J. Li, A. Corma, J. Yu, Chem. Soc. Rev. **44**, 7112–7127 (2015)
4. Y. Li, J. Yu, Chem. Rev. **114**, 7268–7316 (2014)
5. M. Conte, B. Xu, T.E. Davies, J.K. Bartley, A.F. Carley, S.H. Taylor, K. Khalid, G.J. Hutchings, Microporous Mesoporous Mater. **164**, 207–213 (2012)
6. P. Li, W. Zhang, X. Han, X. Bao, Catal. Lett. **134**, 124–130 (2010)
7. M.S. Francesconi, Z.E. Lopez, D. Uzcategui, G. Gonzalez, J.C. Hernandez, A. Uzcategui, A. Loaiza, F.E. Imbert, Catal. Today **107–108**, 809–815 (2005)
8. M.M. Martínez-Iñesta, I. Peral, T. Proffen, R.F. Lobo, Microporous Mesoporous Mater. **77**, 55–66 (2005)
9. A.W. Burton, S.I. Zones, T. Rea, I.Y. Chan, Microporous Mesoporous Mater. **132**, 54–59 (2010)
10. M. Khaleel, A.J. Wagner, K.A. Mkhoyan, M. Tsapatsis, Angew. Chem. Int. Ed. **53**, 9456–9461 (2014)
11. P. Wagner, Y. Nakagawa, G.S. Lee, M.E. Davis, S. Elomari, R.C. Medrud, S.I. Zones, J. Am. Chem. Soc. **122**, 263–273 (2000)
12. W.A. Sławiński, D.S. Wragg, D. Akporiaye, H. Fjellvåg, Microporous Mesoporous Mater. **195**, 311–318 (2014)
13. S. Yang, N.P. Evmiridis, Microporous Mesoporous Mater. **6**, 19–26 (1996)
14. B. Wang, Z. Tian, P. Li, L. Wang, Y. Xu, W. Qu, H. Ma, Z. Xu, L. Lin, Mater. Res. Bull. **44**, 2258–2261 (2009)
15. O. Terasaki, T. Ohsuna, H. Sakuma, D. Watanabe, Y. Nakagawa, R.C. Medrud, Chem. Mater. **8**, 463–468 (1996)
16. G.R. Millward, S. Ramdas, J.M. Thoma, J. Chem. Soc. Faraday Trans. 2 **79**, 1075–1082 (1983)
17. G.T. Kokotailo, N.J. Woodbury, US Patent 4,229, 424 (1979)
18. Y. Song, S. Liu, Q. Wang, L. Xu, Y. Zhai, Fuel Process. Technol. **87**, 297–302 (2006)
19. G.A. Jablonski, L.B. Sand, J.A. Gard, Zeolites **06**, 396–402 (1986)
20. L. Zhang, S. Liu, S. Xie, L. Xu, Microporous Mesoporous Mater. **147**, 117–126 (2012)
21. J. Čejka, A. Corma, S. Zones, *Zeolites and Catalysis: Synthesis, Reactions and Applications* (WILEY-VCH Verlag GmbH & Co. KGaA, Weinheim, 2010), pp. 1–55
22. A. Navrotsky, O. Trofymluk, A.A. Levchenko, Chem. Rev. **109**, 3885–3902 (2009)
23. L.D. Rollmann, J.L. Schlenker, C.L. Kennedy, G.J. Kennedy, D.J. Doren, J. Phys. Chem. B. **104**, 721–726 (2000)
24. C.J. Plank, E.J. Rosinski, M.K. Rubin, US Patent 4,151,189 (1979)
25. M.M.J. Treacy, J.M. Newsam, M.W. Deem, Proc. R. Soc. Lond. A. **433**, 499–520 (1991)
26. Q. Yu, J. Chen, Q. Zhang, C. Li, Q. Cui, Mater. Lett. **120**, 97–100 (2014)
27. S. Mintova, N. Petkov, K. Karaghiosoff, T. Bein, Microporous Mesoporous Mater. **50**, 121–128 (2001)
28. F. Azzolina Jury, I. Polaert, L. Estel, L.B. Pierella, Microporous Mesoporous Mater. **198**, 22–28 (2014)
29. K.P. Dey, S. Ghosh, M.K. Naskar, Mater. Lett. **87**, 87–89 (2012)
30. P.M. Piccione, M.E. Davis, Microporous Mesoporous Mater. **49**, 163–169 (2001)
31. M. Kuman, H. Luo, Y. Roman-Leshkov, J.D. Rimer, J. Am. Chem. Soc. **137**, 13007–13017 (2015)
32. J. Chen, W. Hua, Y. Xiao, Q. Huo, K. Zhu, X. Zhou, Chem. Eur. J. **20**, 14744–14745 (2014)
33. J.B. Nagy, Z. Gabelica, E.G. Derouane, Zeolites **3**, 43–49 (1983)
34. D.T. Hayhurst, A. Nastro, R. Aiello, F. Crea, G. Giordano, Zeolites **8**, 416–422 (1988)
35. O. Larlus, V.P. Valtchev, Chem. Mater. **17**, 881–886 (2005)
36. H. Pan, Q. Pan, Y. Zhao, Y. Luo, X. Shu, M. He, Ind. Eng. Chem. Res. **49**, 7294–7302 (2010)
37. M. Goepper, H.-X. Li, M.E. Davis, J. Chem. Soc. Chem. Commun. **22**, 1665–1666 (1992)
38. V.P. Shiralkar, A. Clearfield, Zeolites **9**, 363–370 (1989)
39. N.Y. Kang, B.S. Song, C.W. Lee, W.C. Choi, K.B. Yoon, Y.-K. Park, Microporous Mesoporous Mater. **118**, 361–372 (2009)
40. P. Sharma, P. Rajaram, R. Tomar, J. Colloid Interfaces Sci. **325**, 547–557 (2008)
41. S.D. Bhat, P.S. Niphadkar, T.R. Gaydhankar, S.V. Awate, A.A. Belhekar, P.N. Joshi, Microporous Mesoporous Mater. **76**, 81–89 (2004)
42. F.J. Machado, C.M. López, M.A. Centeno, C. Urbina, Appl. Catal. A Gen. **181**, 29–38 (1999)
43. S.D. Kim, S.H. Noh, K.H. Seong, W.J. Kim, Microporous Mesoporous Mater. **72**, 185–192 (2004)
44. R. Otomo, T. Yokoi, Microporous Mesoporous Mater. **224**, 155–162 (2016)
45. G. Gonzalez, M.E. Gomes, G. Vitale, G.R. Castro, Microporous Mesoporous Mater. **121**, 26–33 (2009)
46. H. Chen, J. Ding, Y. Wang, New J. Chem. **38**, 308–316 (2014)